DETERMINATION OF STRESS DISTRIBUTION AROUND CIRCULAR TUNNELS USING CONFORMAL MAPPING TECHNIQUE

William E. Green, Industrial Engineering Division, SMMAE,
McClellan Air Force Base

The purpose of this paper is the application of complex variables to a special stress analysis problem. The resolved state of stress is in agreement with what would be expected from the physical geometry of the domain under investigation. The complete investigation is studied as a two-dimensional plane strain problem.

• THE INTENT of this paper is to present an illustrative method using conformal mapping to determine the state of stress surrounding two parallel circular tunnels due to internal pressure loading as shown in Figure 1. The tunnels are cut through an assumed homogeneous and isotropic engineering material that obeys Hooke's Law. The tunnels have parallel longitudinal axes with radii r_1 and r_2, where r_1 is not equal to r_2. The loading in each tunnel is assumed to be an arbitrary normal pressure acting around the whole circumference of the tunnel. To obtain a solution for the state of stress around the tunnels, the geometry of this space is conformally mapped into a finite transformed domain conducive to analytical solution as shown in Figure 2. The problem is then solved analytically in the finite transformed domain for the stress field. These stresses are summed up over arbitrarily small intervals of the transformed space to yield forces that are associated with specified points and directions.

The force vectors with their associative magnitudes, points of action, and directions are then transformed back into the original space to yield an array of oriented forces that are the resultant of the stress distribution in the investigative domain. Using the force array, the state of stress for the investigative domain is thus determined.

NOTATION

a = a constant = 2.906;
$\overline{F}_1$, $\overline{F}_2$ = vectors in the investigative and transformed domains;
ID = investigative domain, Figure 2(a);
$\ell(\phi)$, $\ell(\theta)$ = intervals in the transformed and investigative domains respectively;
p = centerline distance between two tunnels in Figure 3(c);
P_1, P_2 = resultant forces obtained from stresses σ_R and σ_ϕ;
p_j = pressure at a given point or over a given area j;
R, ϕ = a given radius and angle in the annulus, Figure 3(b);
TD = transformed domain, Figure 2(b);
u, v = coordinates in the transformed domain, Figure 3(b);
x, y = coordinates in the investigative domain, Figure 3(a);
θ, a, r;q = angles and radii in the investigative domain, Figure 3(a);
σ_R, σ_ϕ = radial and tangential stresses in annulus, Figure 5;
σ_1, σ_2 = principal stresses in the investigative domain; and
τ_{R_ϕ} = shearing stress in annulus.

Sponsored by Committee on Subsurface–Soil Structure Interaction.

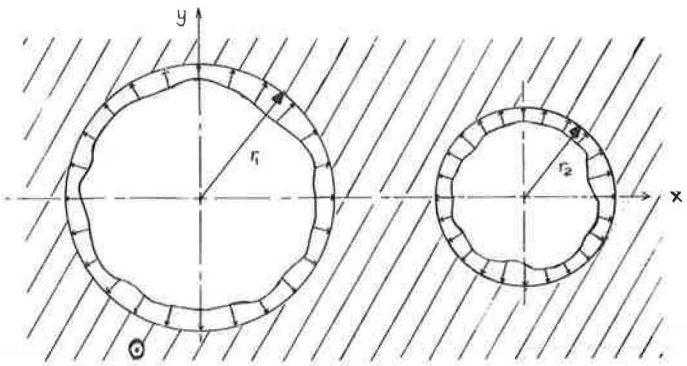

Figure 1. Investigative domain with arbitrary pressure loading.

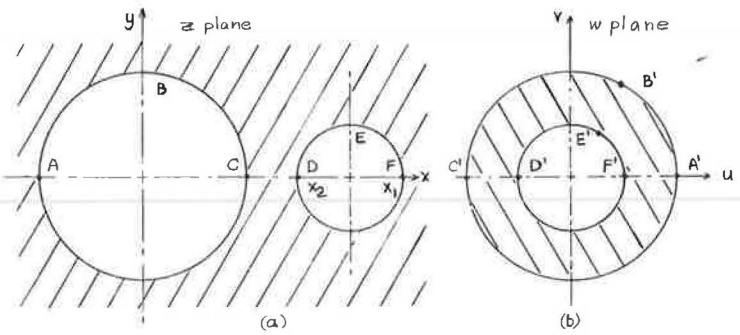

Figure 2. (a) Investigative domain, two-tunnel cross section; (b) transformed domain annulus.

PRELIMINARY CONSIDERATIONS

The determination of the state of stress for the problem with the configuration shown in Figure 1 is accomplished through the utilization of conformal mapping. The purpose of this particular example is to illustrate the technique. All coordinate systems used in this paper are two-dimensional.

To demonstrate the simplicity of the complex variable technique in the solution of the stress analysis problems, the following problem is investigated. Two tunnels of radii r_1 and r_2 ($r_1 \neq r_2$) are considered within an infinite homogeneous, isotropic, linear elastic material; they are subjected to normal loads (pressures) of arbitrary magnitude along their complete circumference. A stress distribution due to this loading is desired around the tunnels. A cross section of this configuration is shown in Figure 1.

The geometry in Figure 1 presents many difficulties that inhibit direct and reasonable solution of the problem leading to a description of the stress field in the domain of interest. Therefore, a conformal mapping transformation is sought that would conformally map the geometry described in Figure 1 into a more convenient geometric cross section that allows the determination of stress distribution over any area of interest.

From Churchill (1, Fig. 16, Appendix 2) the following transformation is written:

$$w = \frac{z - a}{az - 1}; \quad a = \frac{1 + x_1x_2 + \sqrt{(x^2_1 - 1)(x^2_2 - 1)}}{x_1 + x_2} \tag{1}$$

and

$$R_o = \frac{x_1 x_2 - 1 - \sqrt{(x^2_1 - 1)(x^2_2 - 1)}}{x_1 - x_2} \tag{2}$$

where $x_2 < a < x_1$; $0 < R_o < 1$ when $1 < x_2 < x_1$. (See Fig. 2 for a reproduction of Churchill's Fig. 16.)

From Figure 2 and Eq. 1 it is seen that the investigative domain can be mapped conformally into a convenient geometric cross section, i.e., an annulus. From Love (2, p. 144) it is known that the problem of the annulus subjected to boundary loading is readily soluble providing the loading on each boundary is self-equilibrating.

Consider the complex number

$$z = x + iy \tag{3}$$

where $i = \sqrt{1}$. Equation 1 can be written as

$$w = \frac{(x + iy) - a}{a(x + iy) - 1} \tag{4}$$

Separating the real and the imaginary parts yields

$$w = \frac{(x - a)(ax - 1) + ay^2}{(ax-1)^2 + a^2y^2} + i\frac{(a^2 - 1)y}{(ax - 1)^2 + a^2y^2} \tag{5}$$

or

$$w = u + iv = f_5(a,x,y) \tag{5a}$$

where

$$u = \frac{(x - a)(ax - 1) + ay^2}{(ax - 1)^2 + a^2y^2} \tag{6a}$$

and

$$v = \frac{(a^2 - 1)y}{(ax - 1)^2 + a^2y^2} \tag{6b}$$

From Figure 2(b) and Eq. 2 it is deduced that the condition

$$R_o < \frac{1}{a} < 1 \tag{7}$$

must hold if the infinite point is to be included within the annulus, as assumed.

Choosing

$$r_1 = 1 \text{ and } r_2 = \frac{1}{2} \tag{8}$$

in Figure 1 and

$$x_1 = 3.5 \text{ and } x_2 = 2.5 \tag{9}$$

in Figure 2(b) and substituting these values into Eqs. 1 and 2 yields

$$a = 2.906 \tag{10}$$

and

$$R_o = 0.06479 \tag{11}$$

At this point it is easy to check the reciprocal single-valuedness of the selected transformation.

Reviewing Figures 1 and 2, it is noted that all configurations are bounded by circles. Thus, for the sake of convenience Eq. 5 is transformed into polar coordinates.

In polar coordinates,

$$x = r \cos \theta \text{ and } y = r \sin \theta \tag{12}$$

for which Eq. 5 can be written in the form

$$w = \frac{(r \cos \theta - a)(ar \cos \theta - 1) + ar^2 \sin^2 \theta}{(ar \cos \theta - 1)^2 + a^2 r^2 \sin^2 \theta} + i \frac{(a^2 - 1) r \sin \theta}{(ar \cos \theta - 1)^2 + a^2 r^2 \sin^2 \theta} \tag{13}$$

or

$$w = f_6(a, r; \theta) \tag{14}$$

The following identities are noted in Figures 3(a), (b), and (c):

$$\theta + \beta + \gamma = \pi \tag{15}$$

$$\beta = \pi - \alpha = \pi - \theta - \gamma \tag{16}$$

$$\frac{q}{\sin \theta} = \frac{r}{\sin \beta} \tag{17}$$

$$\sin \theta = \frac{q}{r} \sin \alpha = \frac{q \sin \alpha}{\sqrt{p^2 + q^2 + 2pq \cos \alpha}} \tag{18}$$

and

$$\cos \theta = \frac{\sqrt{p^2 + 2pq \cos \alpha + q^2 (1 - \sin^2 \alpha)}}{r} = \frac{p + q \cos \alpha}{\sqrt{p^2 + q^2 + 2pq \cos \alpha}} \tag{19}$$

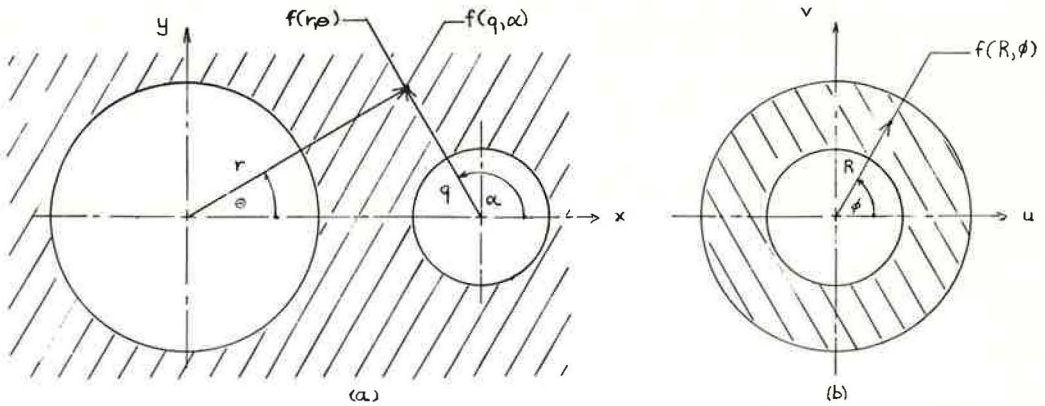

Relations Between Rectangular and Polar Coordinates.

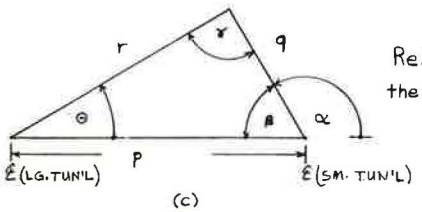

Relations Between Center Lines of the Two Tunnels.

Figure 3. (a and b) Relations between rectangular and polar coordinates; (c) relations between centerlines of the two tunnels.

Substitution of Eqs. 18 and 19 into Eq. 13 yields

$$w = \frac{(p + q\cos\alpha - a)\left[a(p + q\cos\alpha) - 1\right] + aq^2\sin^2\alpha}{\left[a(p + q\cos\alpha) - 1\right]^2 + a^2q^2\sin^2\alpha} + i\,\frac{(a^2 - 1)q\sin\alpha}{\left[a(p + q\cos\alpha) - 1\right]^2 + a^2q^2\sin^2\alpha} \tag{20}$$

or

$$w = f_7(a,p,q;\,\alpha) \tag{20a}$$

For the following specific values,

$$r = 1.000 \tag{21a}$$

$$p = 3.000 \text{ and } q = 0.500 \tag{21b}$$

According to Kantorovich and Krylov (6, p. 36), "Any doubly connected region can be transformed, conformally and with reciprocal single-valuedness, into an annulus with the ratio of the radii of its bounding circumference finite or infinite." This suggests that the two-tunnel configuration [Fig. 2(a)] transforms conformally into the annulus [Fig. 2(b)].

Earlier the loading was defined as normal in direction, arbitrary in magnitude, and acting on the boundaries of the two tunnels in the investigative domain. The arbitrary

character of the loading on the boundaries is selected such that, when transformed into the annulus, it is self-equilibrating on each boundary. The loading on the boundaries of the investigative domain will also be selected so as to permit a convenient loading on the boundaries of the transformed domain.

The specific loading on the annulus (transformed space) is now chosen for ease of solution and for illustration of the technique. One of the most elementary cases of loading and one that yields a well-known elastic solution is that of uniform pressures. This particular case is covered by Wang (4, p. 54).

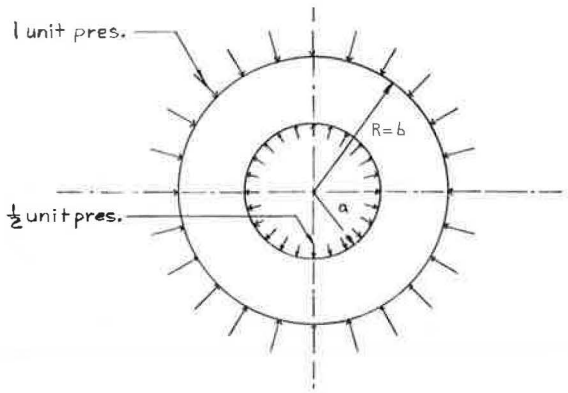

Figure 4. Annulus with loading pressures.

THEORETICAL ANALYSIS

The problem is to determine the state of stress surrounding the two tunnels shown in Figure 2(a). Conformal mapping functions are used to transform the given geometry into a geometry having known solutions. The stress field is calculated for the annulus acted on by the transformed loads, in this case assumed to be uniform pressure on each boundary. The stress values are then cast in suitable form (vectors) for transformation back into the investigative domain. The vector form satisfies the condition that requires invariance with respect to the original and transformed space.

The transformed domain is mapped with its associative, reciprocal, and invariant vector functions back into the investigative domain. Locations and lines of action of the force vectors are also mapped back to the investigative domain. The resulting stress field for the investigative domain is the solution sought.

The transformed domain consists of an annulus with internal and external pressures as shown in Figure 4. The following solution is taken from Timoshenko and Goodier (5, p. 58) with minor modifications. For the boundary conditions

$$\sigma_R = -p_i \text{ at } R = a \tag{22}$$

and

$$\sigma_R = -p_o \text{ at } R = b \tag{23}$$

the stresses are given by the expressions

$$\sigma_R = \frac{a^2b^2(p_o - p_i)}{b^2 - a^2}\frac{1}{r^2} + \frac{p_ia^2 - p_ob^2}{b^2 - a^2} \tag{24}$$

$$\sigma_\theta = \frac{-a^2b^2(p_o - p_i)}{b^2 - a^2}\frac{1}{r^2} + \frac{p_ia^2 - p_ob^2}{b^2 - a^2} \tag{25}$$

$$\tau_{R\phi} = 0 \tag{26}$$

where p_i = internal pressure, p_o = external pressure, a = inside diameter, and b = outside diameter.

Using Eqs. 24 and 25 in conjunction with the following values,

$$p_i = \frac{1}{2},\ p_o = 1 \tag{27}$$

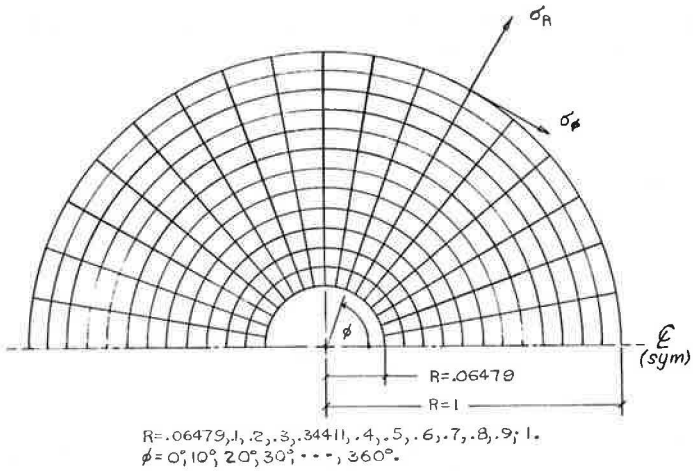

Figure 5. Radial lines and circular arcs superimposed on annulus (top half shown).

$$a = 0.06479 \text{ and } b = 1.00000 \tag{28}$$

the values for the radial and tangential stresses in the annulus can be calculated as given in Table I of the Appendix.[1] Figure 5 shows a network of radial lines and circular arcs. Stresses along the radial lines vary, whereas along the circular arcs these stresses remain constant.

In the following paragraphs the terms investigative domain and two-tunnel cross section with the terms transformed domain and annulus are used interchangeably [Figs. 2(a) and (b)].

Having obtained solutions for the stresses and their distributions in the annulus, it is now necessary to express them in a form that is invariant under transformation. It is known from the theory of vectors that a vector is such an invariant. To facilitate use of this principle, stresses in the annulus may be expressed by equivalent force vectors at a discrete number of points. An axisymmetric dimensional problem permits representation of the forces in the radial and tangential directions for a unit thickness as follows:

$$F_1 = \int_{\phi_1}^{\phi_2} \sigma_R d\ell = \sigma_R \ell(\phi) \tag{29}$$

and

$$F_2 = \int_{\phi_1}^{\phi_2} \sigma_\phi d = \sigma_\phi \ell(\phi) \tag{30}$$

where $\ell(\phi)$ is length. F_1 and F_2 are approximate values. The accuracy of F_1 and F_2 will increase as the value of $|\phi_2-\phi_1|$ decreases.

[1]This paper as originally prepared included an Appendix containing Illustrative Examples I and II, Tables I and II, and Computer Programs for Tables I and II. Because of space limitations, these have not been printed here. This Appendix is available in Xerox form from the Highway Research Board at cost of reproduction and handling. When ordering, refer to XS-36, Highway Research Record 345.

For convenience, each of the circular arcs in the annulus is divided into equal lengths as shown in Figure 5. It follows that

$$\ell(\phi) = \frac{\pi R}{18} \tag{31}$$

Substituting Eq. 31 in Eqs. 29 and 30 yields

$$F_1 = \frac{\pi R \sigma_R}{18} \tag{32}$$

and

$$F_2 = \frac{\pi R \sigma_\phi}{18} \tag{33}$$

F_1 is perpendicular to F_2. Figure 6 is a graphic representation of these force vectors. Values for F_1 and F_2 are given in the Appendix.

Using Eqs. 32 and 33, σ_R and σ_ϕ values are summed along the contours and are defined as F_1 and F_2. These forces are assumed located at the geometric center points of the intervals. This summation redefines the stresses as an array of forces having location, magnitude, and direction, as shown in Figure 6(b). It is possible to shift all F_1 and F_2 forces, located at the center point of the intervals, to the intersection points of the intervals. This rotation along the circular arcs is shown in Figure 7.

Each of the F_1 and F_2 forces has an associative point location and a directional angle. The force quantities are now written as, $\overline{F}_1$ and $\overline{F}_2$, where the quantity is a vector. In the annulus there exists an array of force vectors located at the intersection of the radial lines and circular arcs. The point angle relationship is in general uniquely maintained under conformal transformation (6, Theorems 1 and 2, pp. 626 and 628). Consequently, the force vectors, $\overline{F}_1$ and $\overline{F}_2$, after transformation maintain the same point-angle relationship that they held in the original space.

Writing the force vectors, $\overline{F}_1$ and $\overline{F}_2$, in a general form for the annulus,

$$\overline{F}_1 = \overline{F}\left[P_1, f(u,v); \phi(u,v)\right] \tag{34}$$

and

$$\overline{F}_2 = \overline{F}\left[P_2, f(u,v); \phi(u,v) + 90^0\right] \tag{35}$$

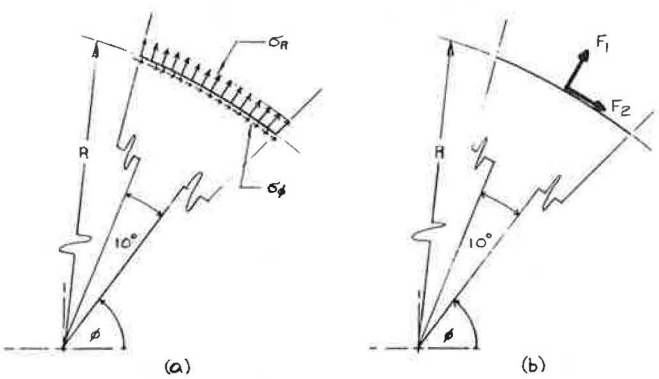

Figure 6. (a) Representations of σ_R and σ_ϕ acting along a 10-deg interval of an arc; (b) F_1 and F_2 force vectors acting through a center point of the interval of arc.

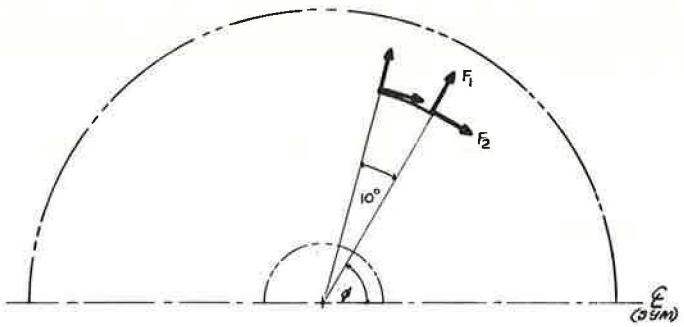

Figure 7. Transition of force vectors to intersection points on the circumferential curve.

where

P_1, P_2 = resultant forces obtained from the stresses (36)

$f(u,v)$ = a nodal point through which $\overline{F}_1$ and $\overline{F}_2$ act in the w plane (37)

$\phi(u,v)$ = the angle between the line of action of $\overline{F}_1$ and the u-axis of the w plane (38)

and

$\phi(u,v) + 90°$ = the angle between the line of action of $\overline{F}_2$ and the u-axis of the w plane (39)

It is observed that under transformation, Eq. 36 remains constant, while Eqs. 37, 38, and 39 undergo transformation. Conformally mapping Eqs. 37, 38, and 39, in a general form, into the original space (investigative domain) yields

$$f(u,v) \rightarrow f(x,y)$$

and

$$\phi(u,v) \rightarrow \psi(x,y)$$

where $f(x,y)$ and $\psi(x,y)$ define the nodal points and directional angles associated with the investigative domain. Consequently, a general definition of the transformed vector pair, $\overline{F}_1$ and $\overline{F}_2$, in the investigative domain, is written as follows:

$$\overline{F}_1 = \overline{F}\left[P_1, f(x,y); \psi(x,y)\right] \tag{40}$$

and

$$\overline{F}_2 = \overline{F}\left[P_2, f(x,y); \psi(x,y) + 90°\right] \tag{41}$$

where

$f(x,y)$ = a nodal point through which $\overline{F}_1$ and $\overline{F}_2$ act in the z plane (42)

$\psi(x,y)$ = the angle between the line of action of $\overline{F}_1$ and the x-axis in the z plane (43)

and

$\psi(x,y) + 90°$ = the angle between the line of action of $\overline{F}_2$ and the x-axis in the z plane (44)

From Kantorovich and Krylov (3, p. 36), the principle of "reciprocal single-valuedness" is now invoked for the original transformation given by Eq. 1, in which z is written in terms of w to yield

$$z = \frac{w - a}{aw - 1} = \frac{(u - a)(au - 1) + av^2}{(au - 1)^2 + a^2v^2} + i\frac{(a^2 - 1)v}{(au - 1)^2 + a^2v^2} \tag{45}$$

Using the polar relationships,

$$u = R\cos\phi \tag{45a}$$

$$v = R\sin\phi \tag{45b}$$

Eq. 45 is now written

$$z = \frac{(R\cos\phi - a)(aR\cos\phi - 1) + aR^2\sin^2\phi}{(aR\cos\phi - 1)^2 + a^2R^2\sin^2\phi} + i\frac{(a^2 - 1)R\sin\phi}{(aR\cos\phi - 1)^2 + a^2R^2\sin^2\phi} \tag{46}$$

Equation 46 may also be expressed in the form

$$z = x + iy = f(a,R;\phi) \tag{47}$$

where

$$x = \frac{(R\cos\phi - a)(aR\cos\phi - 1) + aR^2\sin^2\phi}{(aR\cos\phi - 1)^2 + a^2R^2\sin^2\phi} \tag{48}$$

and

$$y = \frac{(a^2 - 1)R\sin\phi}{(aR\cos\phi - 1)^2 + a^2R^2\sin^2\phi} \tag{49}$$

Note that $R = |w| = \sqrt{u^2 + v^2}$ and $|z| = \sqrt{x^2 + y^2}$.

In the transformed domain each point of intersection is a nodal point associated with the vector pair, $\overline{F}_1$ and $\overline{F}_2$, and the corresponding directional angles $\phi(u,v)$ and $\phi(u,v) + 90$ deg. Now invoking the principle of "reciprocal single-valuedness" it can be assumed that a similar relationship to that in the transformed domain will exist in the investigative domain. Therefore, in the investigative domain at each intersection point (x,y) there exist force vectors, $\overline{F}_1$ and $\overline{F}_2$, with the directional angles $\psi(x,y)$ and $\psi(x,y) + 90$ deg.

Equation 46 can be written as

$$z = z_n(a,R;\phi) = z_n(x,y) \tag{50}$$

where n identifies a specific subset of transformed points selected from the annulus at a given radius R. Equation 50 yields a complete set of equations describing all transformed points of intersection (nodal points) as follows:

$$z_1(a,R = 0.06479;\ \phi = 0, 10, 20, \ldots 360 \text{ deg}) \tag{50a}$$
$$z_2(a,R = 0.1;\ \phi = 0, 10, 20, \ldots 360 \text{ deg}) \tag{50b}$$
$$z_3(a,R = 0.2;\ \phi = 0, 10, 20, \ldots 360 \text{ deg}) \tag{50c}$$
$$z_4(a,R = 0.3;\ \phi = 0, 10, 20, \ldots 360 \text{ deg}) \tag{50d}$$

$$z_5(a,R = 0.34411;\ \phi = 0,10,20,\ldots 360 \text{ deg}) \quad (50e)$$
$$z_6(a,R = 0.4;\ \phi = 0,10,20,\ldots 360 \text{ deg}) \quad (50f)$$
$$z_7(a,R = 0.5;\ \phi = 0,10,20,\ldots 360 \text{ deg}) \quad (50g)$$
$$z_8(a,R = 0.6;\ \phi = 0,10,20,\ldots 360 \text{ deg}) \quad (50h)$$
$$z_9(a,R = 0.7;\ \phi = 0,10,20,\ldots 360 \text{ deg}) \quad (50i)$$
$$z_{10}(a,R = 0.8;\ \phi = 0,10,20,\ldots 360 \text{ deg}) \quad (50j)$$
$$z_{11}(a,R = 0.9;\ \phi = 0,10,20,\ldots 360 \text{ deg}) \quad (50k)$$
$$z_{12}(a,R = 1.0;\ \phi = 0,10,20,\ldots 360 \text{ deg}) \quad (50l)$$

This set of equations represents a map of the intersection points (nodal points) for the investigative domain. If the points defined by Eq. 50 are joined by a free curve, a map (as shown in Fig. 8) results that represents the transformed radial lines and circular arcs. The directional angles, $\psi(x,y)$ and $\psi(x,y) + 90$ deg, may be obtained by determining the normal and tangent to the transformed circular arcs—R curves in Figure 8—at the point of interest. It may be of interest to note that the force vectors, $\overline{F}_1$ and $\overline{F}_2$, act normal and tangential to the curves in both the investigative and transformed domains.

Figure 9 shows some typical vectors $\overline{F}_1$ and $\overline{F}_2$ located at various points of intersection in the investigative domain. Note: $\overline{F}_1$ is rotated 180 deg in direction at the transformed radial point R = 0.34411 defining the infinite point in the investigative domain. A complete picture of the loading apposite to the investigative domain will show $\overline{F}_1$ and $\overline{F}_2$ vectors located at each point of intersection in Figure 9.

In summary:

1. The stresses, σ_R and σ_ϕ, belonging to the transformed domain have been resolved into force vectors, $\overline{F}_1$ and $\overline{F}_2$.
2. The magnitude, location and lines of action of the vector pair have been defined in the transformed domain.
3. The vector pair, $\overline{F}_1$ and $\overline{F}_2$, have been transformed into the investigative domain in which their magnitude, location, and lines of action have been defined.

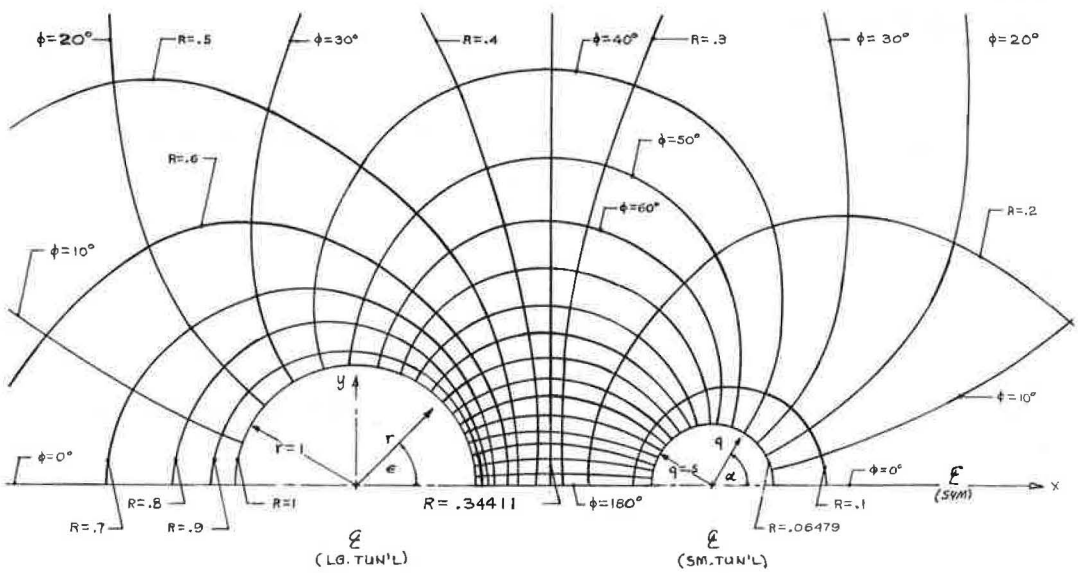

Notes:
1. x, y, r, θ, q and α indicate the Rectangular and Polar Coordinates revelant to the Investigative Domain.
2. R and φ indicate the Transformed Radial Lines and Circular Arcs

Figure 8. Transformed radial lines and circular arcs.

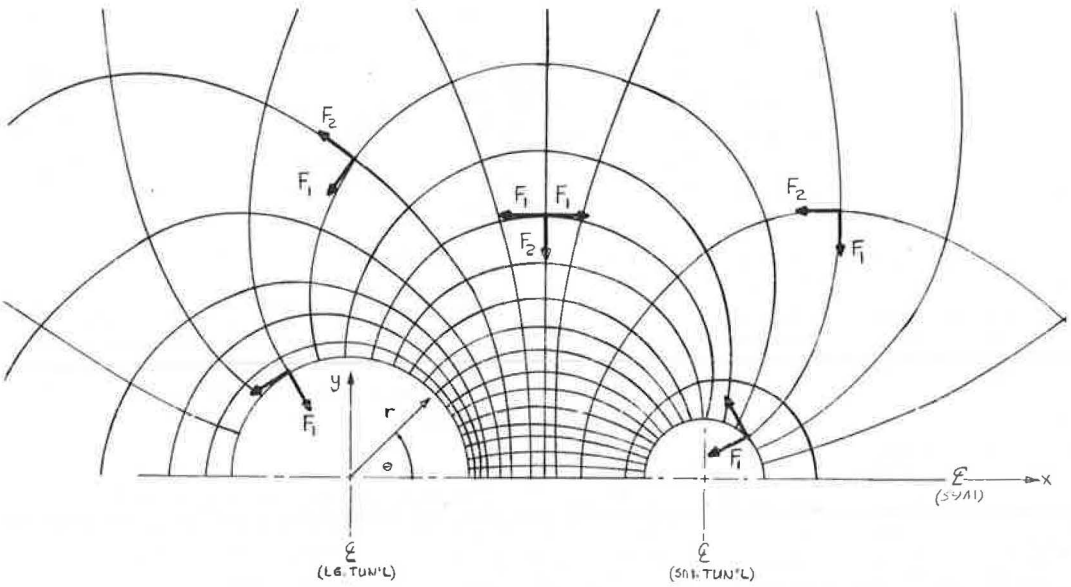

Figure 9. F_1 and F_2 shown at different intersection points in the investigative domain.

It is now possible to describe the stresses in the investigative domain. In the transformed domain the circumferential curves are divided into equal intervals for each given R (Fig. 5), and the stresses are summed over these intervals to yield the vector quantities, $\overline{F}_1$ and $\overline{F}_2$.

Examination of Figure 8 reveals that the transformed intervals assume differing lengths.

Recalling Eqs. 29 and 30, and noting that

$$\ell(\phi) \rightarrow \ell(\sigma)$$

i.e., $f(\phi)$ yields $f(\theta)$ under transformation, the following expressions result:

$$\sigma_1 = \frac{F_1}{\ell(\phi)} \tag{51}$$

and

$$\sigma_2 = \frac{F_2}{\ell(\phi)} \tag{52}$$

In Eqs. 51 and 52, σ_1 and σ_2 are the principal stresses in the investigative domain, where

$$\overline{F}_{1,2} = \left|F_{1,2}\right| \tag{53}$$

and $\ell(\phi)$ is the corresponding interval length in the investigative domain.

In this case the principal stresses σ_1 and σ_2 act in directions normal and tangent to the transformed circular arcs, $R = R_i$, in Figure 8. It is known from the study of stress analysis that the state of stress at any point is completely determined by the magnitude and direction of the two principal stresses.

An approximation for $\ell(\theta)$ is obtained from

$$\ell(\theta) = |z_m - z_{m+1}| + |z_{m+2}| + \cdots + |z_{m+9} - z_{m+10}|$$

$$= \sum_{k=m}^{m+9} |z_k - z_{k+1}| \tag{54}$$

where z_k is defined by Eq. 50 with the following changes:

$$m = \phi = 0, 10, 20, \ldots 350 \text{ deg} \tag{55}$$

i.e., k indicates the actual degree value at which z_k is evaluated.

The accuracy of the principal stresses, σ_1 and σ_2, in the investigative domain is dependent on the length $\ell(\phi)$.

Defining the polar coordinates for all points in the investigative domain, it follows that

$$r = |z| \tag{56}$$

and

$$\theta = \text{Arctan } (y/x) \tag{57}$$

where z, x and y are defined by Eqs. 46, 48, and 49 respectively. Consequently, the principal stresses, σ_1 and σ_2, with associative polar coordinates may be determined.

The equations define x, y, r, θ, and σ_1 and σ_2 in the investigative domain at locations indicated in both rectangular and polar coordinates. Each coordinate location in the table represents the common point to the two adjacent intervals. The distance between any two consecutive points is written in the complex form $|z_j - z_{j+1}|$. In Appendix Table II, ℓ represents the approximate distance along the transformed curve between z_j and z_{j+1}. In the table, the principal stresses, $(\sigma_1)_j$ and $(\sigma_2)_j$, represent average values over an interval defined by (x_j, y_j) and (x_{j+1}, y_{j+1}). The stresses σ_1 and σ_2 are taken constant over this interval ℓ. Also included in the table are the related values of R and ϕ indicating the location in the transformed domain. F_1 and F_2 are constant in both domains.

Two examples using Table II and Figure 8 are included in the Appendix.

Earlier, the investigative domain's boundary loading is defined arbitrarily. For convenience of calculation, the loadings selected in this paper are those that, when transformed to the annulus, permit easy solution and satisfy the condition of being self-equilibrating.

Consider first the case of the large tunnel (Fig. 8), r = 1. From Appendix Table II-L, the stresses σ_1 and σ_2 and the interval $\ell(\theta)$ over which they act are readily determined. Each interval $\ell(\theta)$ on the boundary of the large tunnel is a circular arc having a specific constant value of stress. It is assumed that a uniform pressure, p_j, acts on the outer boundary of each interval, equal in intensity to the stress, $(\sigma_1)_j$. It is noted that σ_1 acts normal to the boundaries, r = 1 and q = 1/2 in Figure 8. For the large tunnel the beginning and end points of the intervals are defined:

$$r = r_1 = 1.0 \tag{58}$$

and

$$\theta = \theta_1, \theta_2, \theta_3, \ldots \tag{59}$$

The values of θ_j are given in Appendix Table II-L. At the boundary of the large tunnel $\theta(x,y) = \psi(x,y)$.

Consideration of the small tunnel leads to the same conclusions except that (a) the stress σ_1 and the interval $\ell(\theta)$ are taken from Appendix Table II-A and (b) the beginning and end points of an interval, z_j and z_{j+1}, are defined as follows:

$$q = q_1 = \frac{1}{2} \tag{60}$$

and

$$\alpha = \alpha_1, \alpha_2, \alpha_3, \ldots \tag{61}$$

where

$$\alpha = \text{Arccos}\,(2x - 6) \tag{62}$$

in which x is determined by Eq. 48. At the boundary of the small tunnel $\alpha(x,y) = \psi(x,y)$.

Figure 10 shows a plot of the loadings on the top half of the boundaries of the two tunnels. Figure 10(a) is constructed by using σ_1 and θ values from Appendix Table II-L.

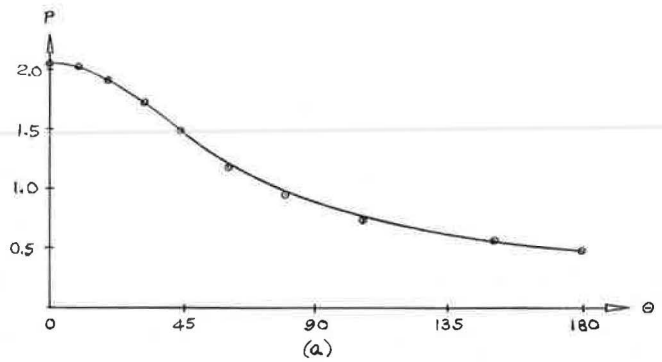

Pressure Loading on Boundary of Large Tunnel

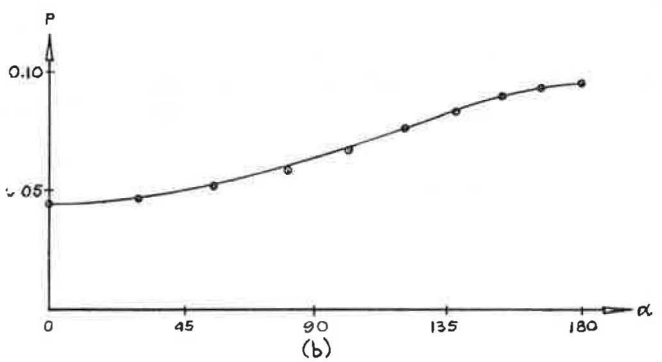

Pressure Loading on Boundary of Small Tunnel

Note: σ_1 is Equal and Opposite to the Normal Pressure

Figure 10. Normal pressure distribution on the boundaries, investigative domain.

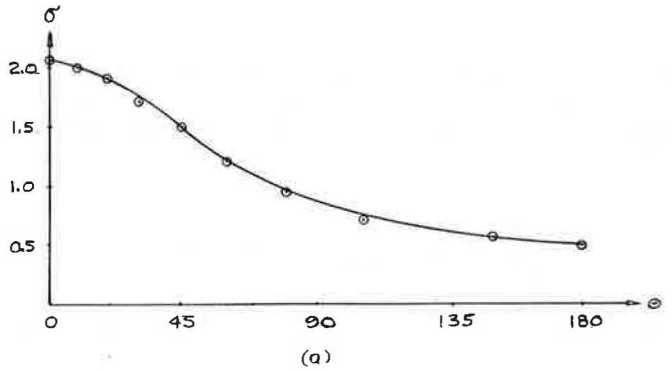

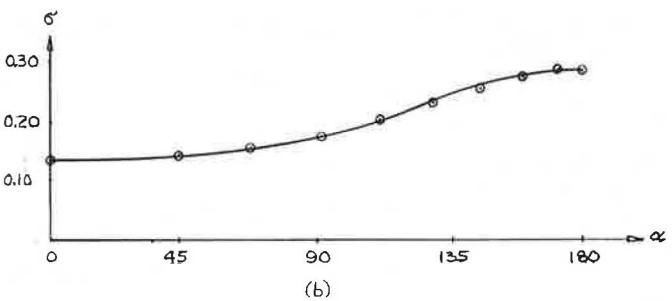

Figure 11. σ_2 distribution on the boundaries of the investigative domain.

Figure 10(b) is a combination of σ_1 and x values from Appendix Table II-A in conjunction with Eq. 62. Principal stress σ_1 is equal and opposite in intensity to the boundary loadings.

The distribution of the tangential stress σ_2 on the boundaries of the investigative domain is shown in Figure 11.

CONCLUSIONS

The intent of this paper is to illustrate a method by which the technique of conformal mapping is used as a vehicle in the determination of the state of stress surrounding the two tunnels as shown in Figure 1. In Appendix Table II, the principal stresses, σ_1 and σ_2, with the associated intervals over which these values are considered constant, are given. The beginning and end points of the intervals coincide with the points of intersection on the transformed circular arcs. The actual path of the intervals can be determined analytically from the transformation equations.

Figure 8 shows the transformed radial lines and circular arcs in the immediate area surrounding the two tunnels. The path of the intervals is established graphically by tracing the path of the transformed circular arcs, i.e., the R-curves in Figure 8.

The principal stresses σ_1 and σ_2 act in normal and tangential direction respectively to the intervals $\ell(\theta)$.

The loadings on the two tunnels are segmented uniform normal pressures equal to the boundary stresses σ_1 given in Appendix Tables II-A and II-L. For instance, a uniform pressure p_j acts over the interval $\ell_j(\theta)$ associated with stress $(\sigma_1)_j$, such that

$$p_j = (\sigma_1)_j \tag{63}$$

where p_j acts uniformly over the interval $\ell_j(\theta)$ for which the stress $(\sigma_1)_j$ on the boundaries of the investigative domain is constant. Figure 10 shows a distribution of the loadings and σ_1 stresses on the boundaries of the investigative domain. Similarly, the distribution of σ_2 stresses on the boundaries of the investigative domain are shown in Figure 11.

Primary consideration in this paper is given to the technique of solution. For practical application of the results, consider Figure 10 and Eq. 63, from which loading diagrams for the tunnels can be constructed. These diagrams then determine the acceptable external load arrangement for the tunnels.

REFERENCES

1. Churchill, R. V. Complex Variables and Applications. McGraw-Hill Book Co., Inc., New York, 1960.
2. Love, A. E. H. A Treatise on the Mathematical Theory of Elasticity, 4th Ed. Dover Publications, New York, 1927.
3. Kantorovich, L. H., and Krylov, V. I. Approximate Methods of Higher Analysis. Interscience Publishers Inc., New York, 1958.
4. Wang, C. T. Applied Elasticity. McGraw-Hill Book Co., Inc., New York, 1953.
5. Timoshenko, S., and Goodier, J. N. Theory of Elasticity. McGraw-Hill Book Co., Inc., New York, 1951.
6. Wylie, C. R. Advance Engineering Mathematics. McGraw-Hill Book Co., Inc., New York, 1960.